This paper describes objective technical results and analysis. Any subjective views or opinions that might be expressed in the paper do not necessarily represent the views of the U.S. Department of Energy or the United States Government.

SAND2018-8875C

Advanced Model Predictions of Mechanical Properties and Process Parameter Effects in High Throughput L-PBF Tension Specimens

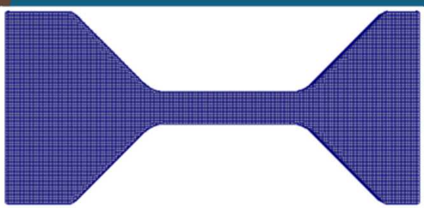

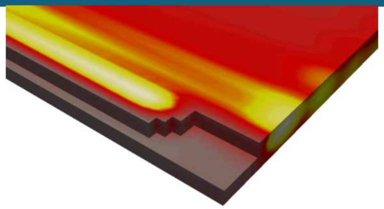

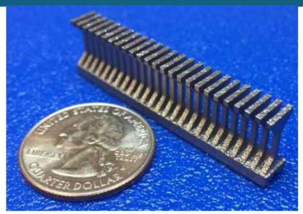

PRESENTED BY

Kyle Johnson, Laura Swiler, Theron Rodgers, Bradley Jared, Sam Subia, Kurtis Ford, Mike Stender, and Joe Bishop

Sandia National Laboratories is a multimission laboratory managed and operated by National Technology & Engineering Solutions of Sandia, LLC, a wholly owned subsidiary of Honeywell International Inc., for the U.S. Department of Energy's National Nuclear Security Administration under contract DE-NA0003525.

Outline

Background

Thermal Modeling and Solid Mechanics Modeling in Sierra

Dogbone Gage Section Models

Mechanical Property Predictions

Laser Parameter Study

Conclusions and Future Work

AM Can Produce Extreme Properties

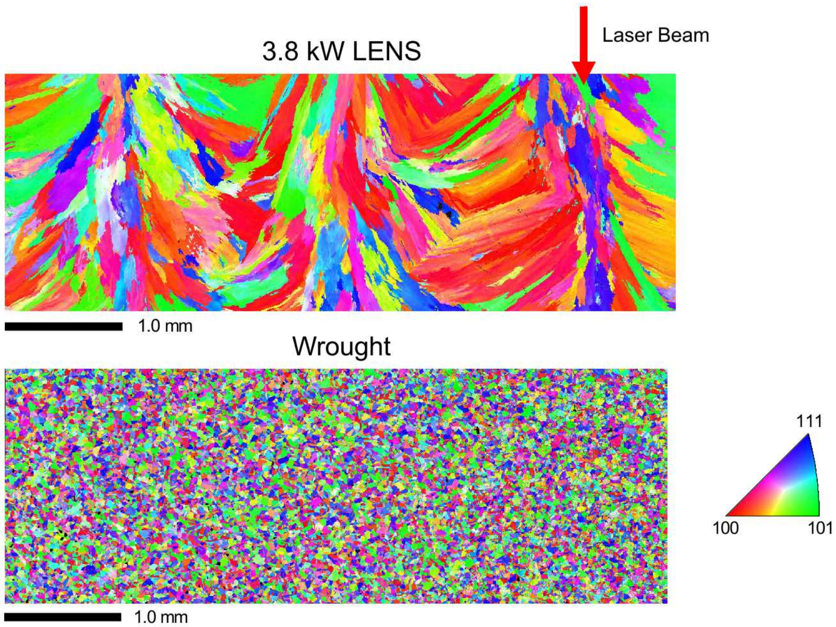

(J. Michael, SNL)

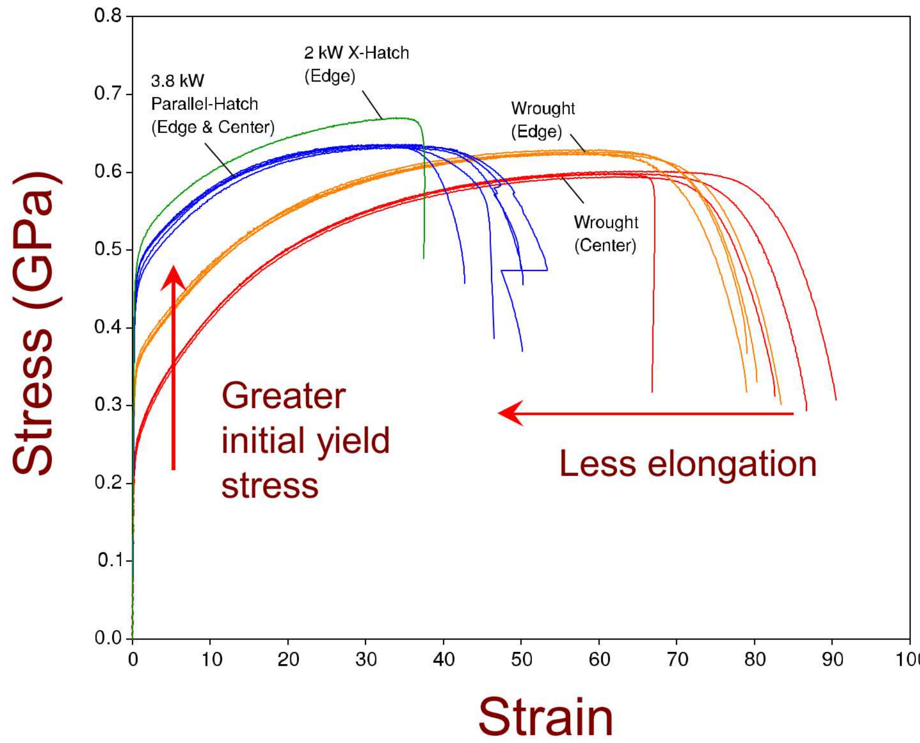

(J. Carroll, SNL)

- 304L Stainless Steel

High Thermal Gradients Produce High Residual Stresses

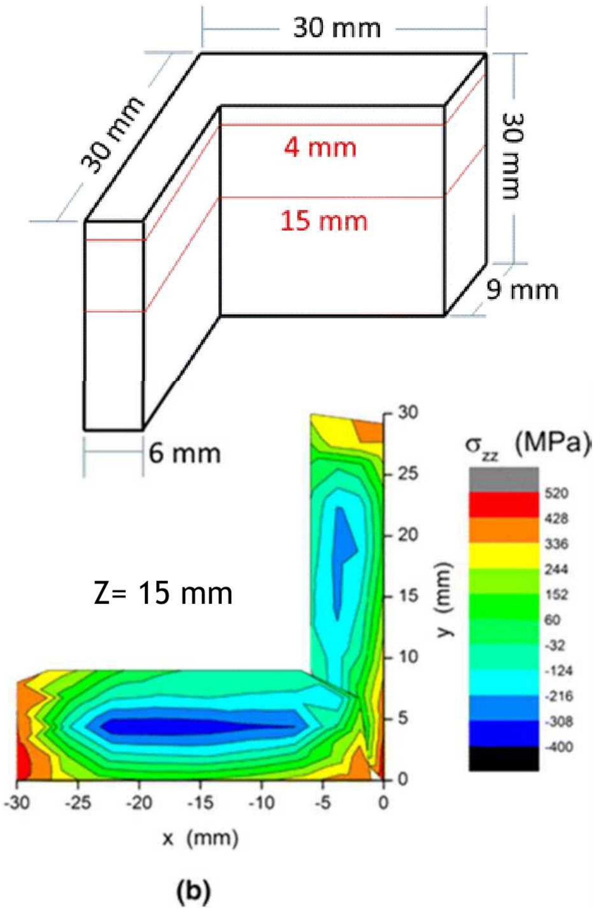

316L Stainless Steel Powder Bed
Wu *et al.* 2014 (LLNL, LANL)

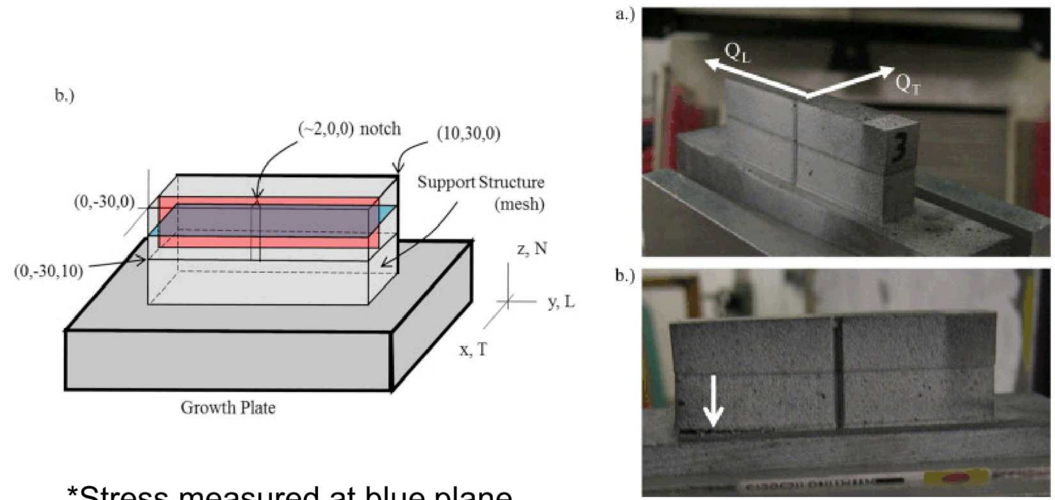

*Stress measured at blue plane

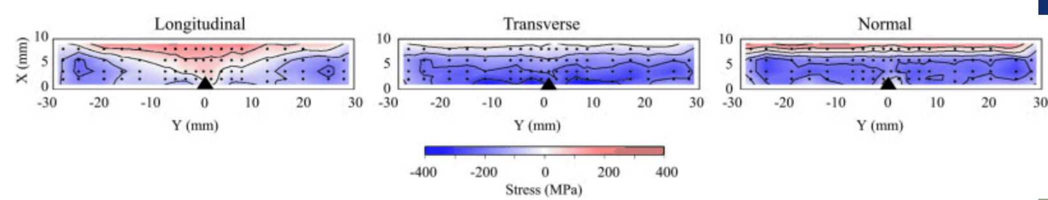

17-4 Stainless Steel Powder Bed
Brown *et al.* 2016 (LANL)

AM Materials Exhibit Higher Dislocation Density

Brown *et al. 2017, Met Trans A*

Table III. Microstructural Parameters Determined from DLPA

Sample	T/C geometry	Applied Strain	X_A (nm)	$\rho \times 10^{14}$ (1/m^2)	M
W–U	C	0	[illegible]	0.13 (3)	
W–U	T	0	[illegible]	0.30 (3)	
P–U	C	0	[illegible]	2.4 (2)	2.25
P–U	T	0	[illegible]	2.4 (2)	2.14
X–U	C	0	[illegible]	1.2 (1)	3.50
X–U	T	0	[illegible]	1.5 (1)	3.73
W–C	[illegible]	[illegible]	[illegible]	[illegible]	3.03
P–C	[illegible]	[illegible]	[illegible]	[illegible]	1.86
X–C	[illegible]	[illegible]	[illegible]	[illegible]	2.29
W–T	[illegible]	[illegible]	[illegible]	[illegible]	1.49
P–T	[illegible]	[illegible]	[illegible]	[illegible]	1.32
X–T	[illegible]	[illegible]	[illegible]	[illegible]	1.61

W [illegible]

Wrought 304L

LENS 304L

Can we predict the higher yield caused by increased dislocation density?

Smith *et al. 2018, JOM*

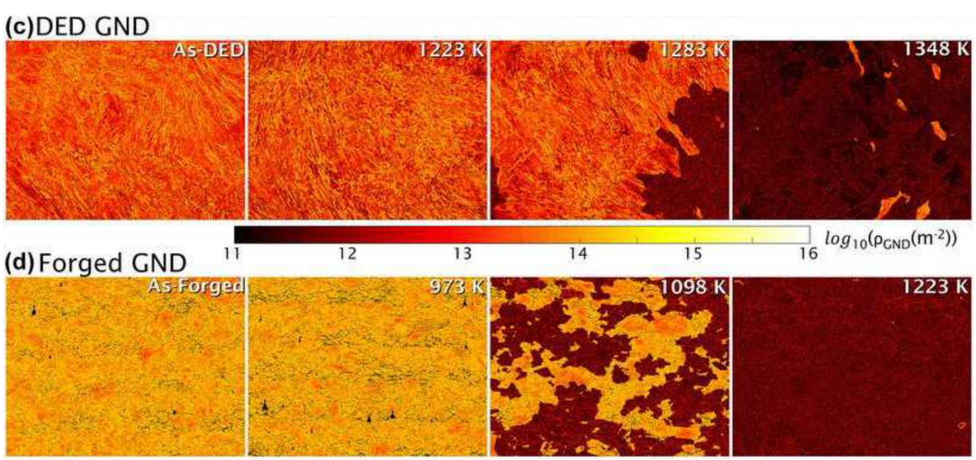

Thermal Approach

Pre-meshed part is initialized with "inactive" elements. Baseplate elements are active.

Laser heat source is scanned according to input path

Elements are activated by a thermal conductivity increase once they reach melt temperature

Conduction, convection, and radiation are considered.

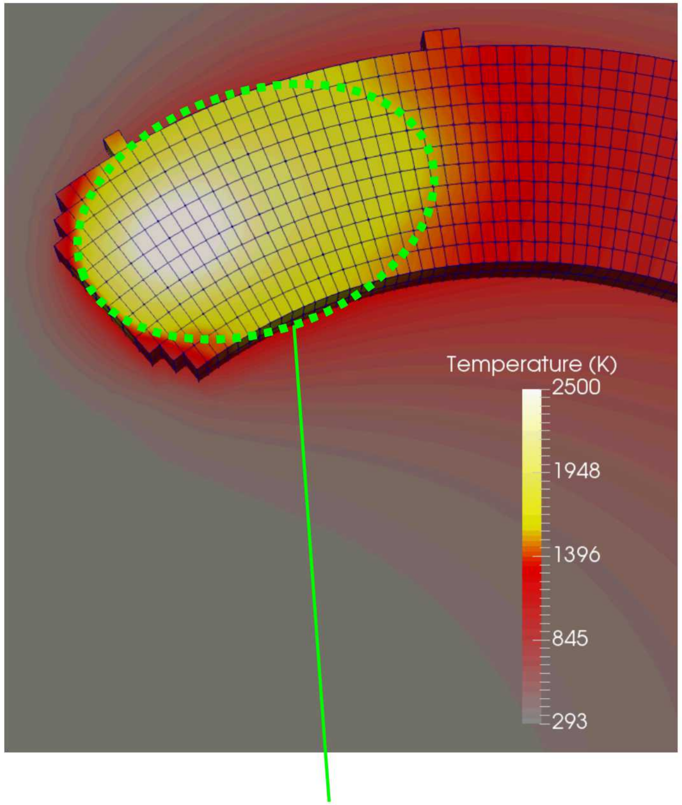

Approximate Melt Pool

Solid Mechanics Approach

Pre-meshed part is initialized with "inactive" elements. Baseplate elements are active.

Thermal output file is read at every time step to provide temperatures

Elements are activated once they reach melt temperature

Residual stress builds as elements contract upon cooling and build thermal strain

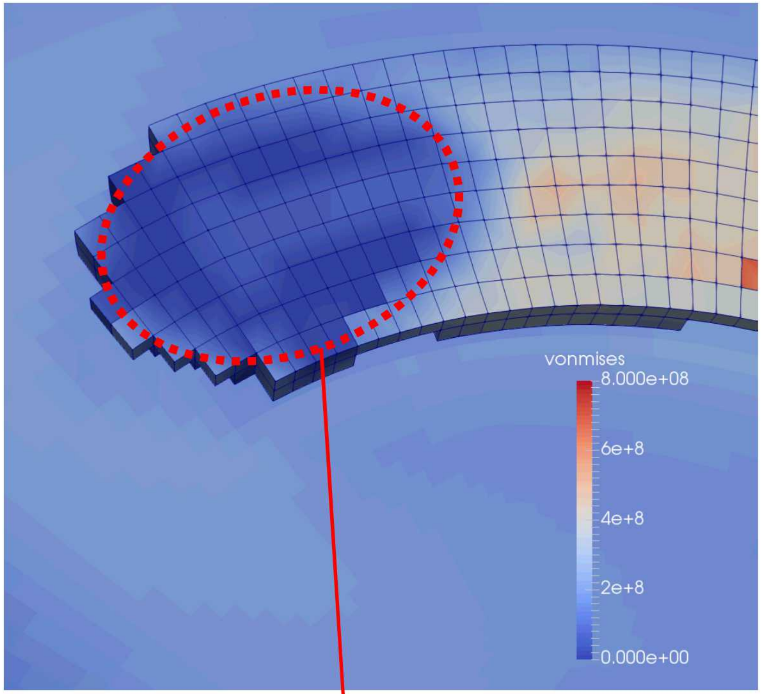

Approximate Melt Pool
(~zero stress)

Bammann-Chiesa-Johnson (BCJ) Material Model

- Temperature and history-dependent viscoplastic internal state variable model
- Stress is dependent on damage ϕ and evolves according to

$$\dot{\sigma} = \left(\frac{\dot{E}}{E} - \frac{\dot{\phi}}{1-\phi}\right)\sigma + E(1-\phi)(\dot{\varepsilon} - \dot{\varepsilon}_p)$$

- Flow rule includes yield stress and internal state variables for hardening and damage

$$\dot{\varepsilon}_p = f\,sinh^n\left(\frac{\frac{\sigma_e}{1-\phi} - \kappa}{Y} - 1\right)$$

- Statistically stored dislocations are represented by isotropic hardening variable κ

$$\kappa = c_{\varepsilon_{ssds}} b\mu(\theta)\sqrt{\rho_{ssds}} \qquad \dot{\rho}_{ssds} = \left[\frac{k_1}{L_s} + \frac{k_2}{L_g} - R_d(\theta)\rho_{ssds}\right]\dot{\varepsilon}_p$$

- The isotropic hardening variable κ evolves in a hardening minus recovery form.

$$\dot{\kappa} = \kappa\frac{\dot{\mu}}{\mu} + (H(\theta) - R_d(\theta)\kappa)\dot{\varepsilon}_p$$

- Geometrically necessary dislocations are represented by a misorientation variable ζ

$$\dot{\zeta} = \frac{\zeta}{\mu(\theta)}\frac{d\mu}{d\theta}\dot{\theta} + h_\zeta\mu(\theta)\left(\frac{\zeta}{\mu(\theta)}\right)^{1-\frac{1}{r}}|\dot{\varepsilon}_p|$$

(Bammann *et al.* 1993, Brown and Bammann 2012)

Incorporating porosity as initial damage

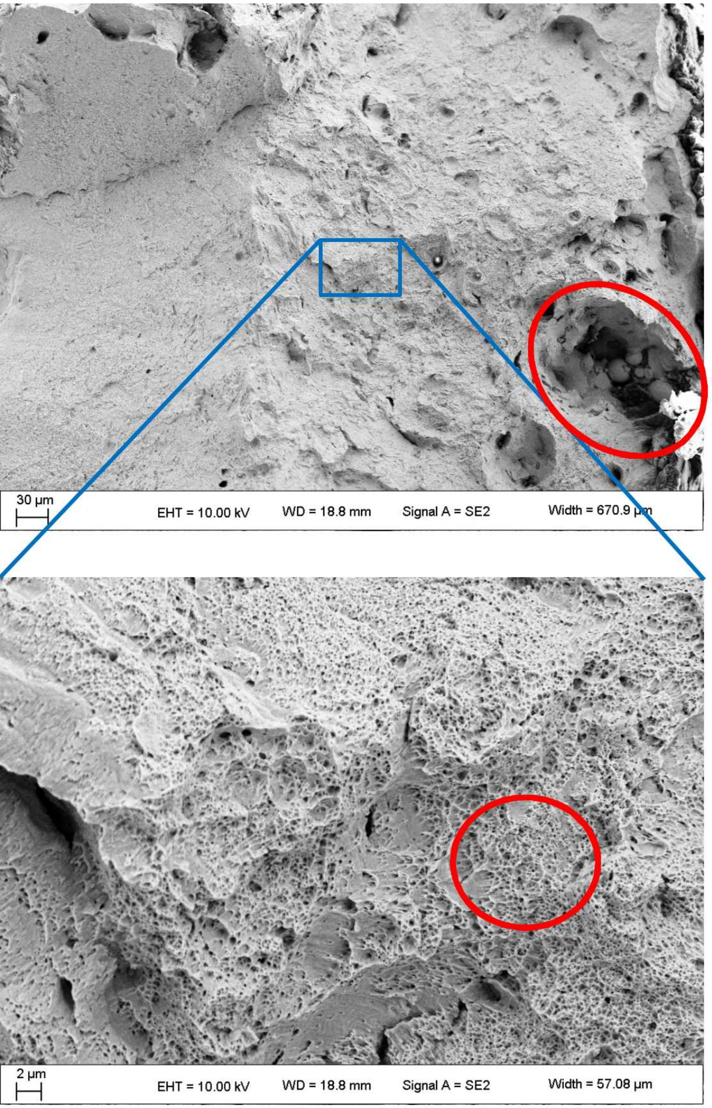

Void Growth

Pre-existing voids captured by void growth

$$\dot{\phi} = \sqrt{\frac{2}{3}}\dot{\epsilon}_p \frac{1-(1-\phi)^{m+1}}{(1-\phi)^m} \sinh\left[\frac{2\,(2m-1)}{2m+1}\frac{\langle p \rangle}{\sigma_e}\right]$$

Void Nucleation

Fine scale voids (< 1μm) indicate nucleation

$$\dot{\eta} = \eta\dot{\epsilon}_p \left(N_1 \left[\frac{4}{27} - \frac{J_3^2}{J_2^3}\right] + N_2 \frac{J_3}{J_2^3} + N_3 \frac{\langle p \rangle}{\sigma_e} \right)$$

*Fractography taken from 3rd Sandia Fracture Challenge

LPBF High Throughput Dogbone Example

Process	Structure	Property	Performance
Thermal and Structural Model (Scan path, laser power, laser speed)	Initial dislocation density, defects	Residual Stress, Higher yield, UTS	Component behavior using as-built properties, residual stress, and porosity

- Laser diameter = 120 μm
- Laser Speed = 1400 mm/s
- Layer Thickness = 0.03 mm
- Laser Power = 120 W
- Hatch Spacing = 60 μm
- Material model calibrated to wrought data

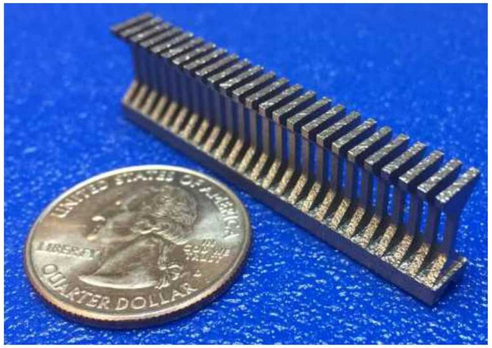

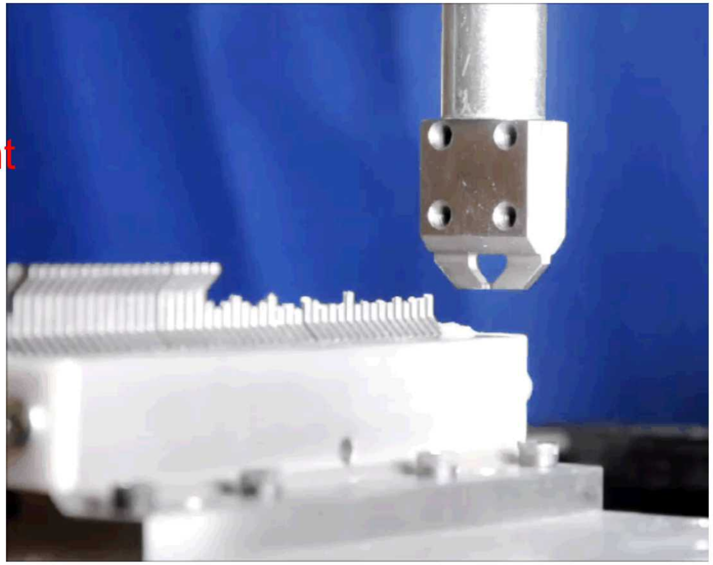

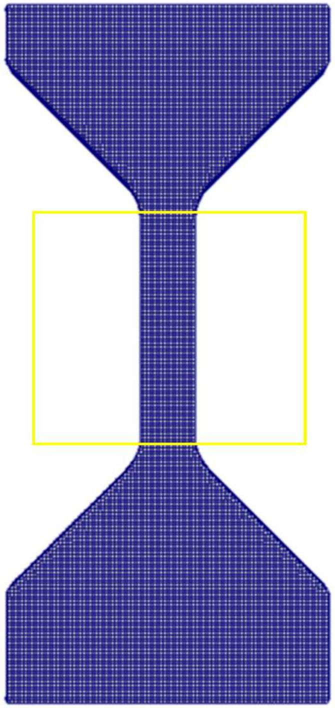

Thermal and Structural Results

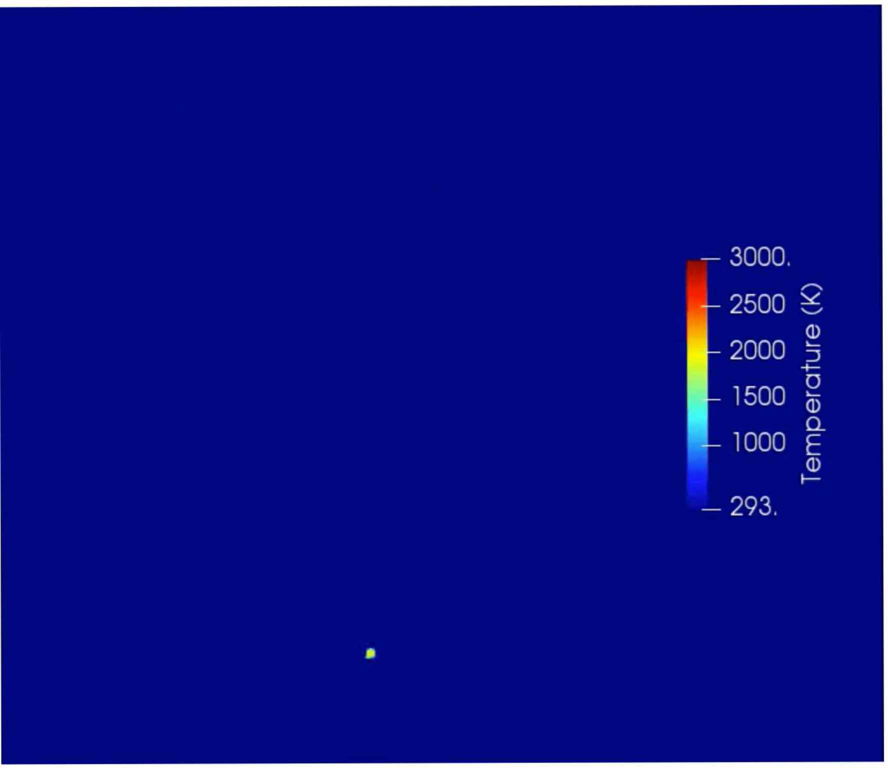

Thermal

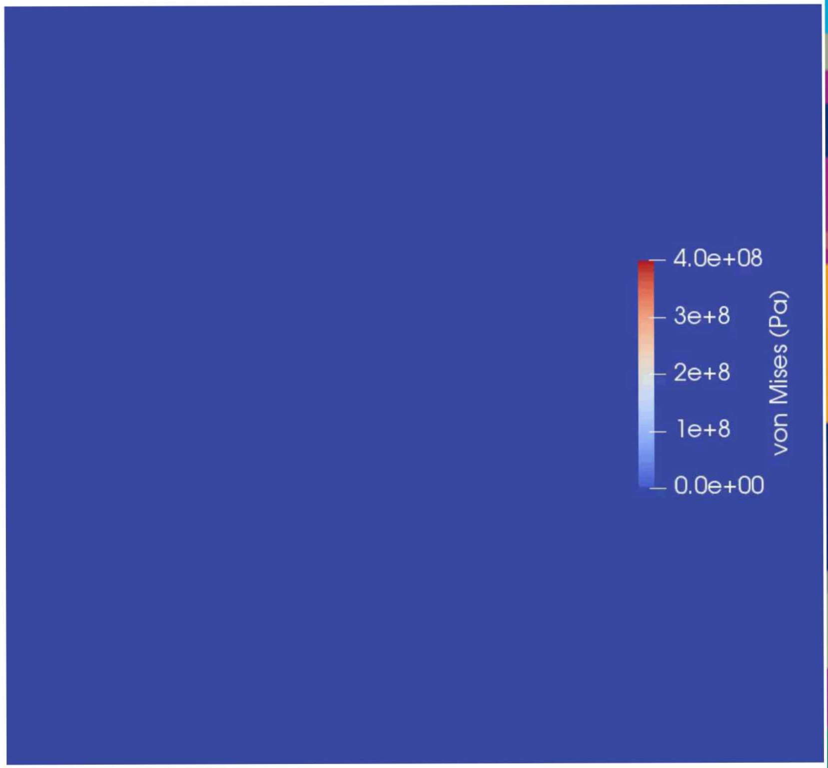

Structural

Significant Tensile and Compressive Residual Stresses Remain

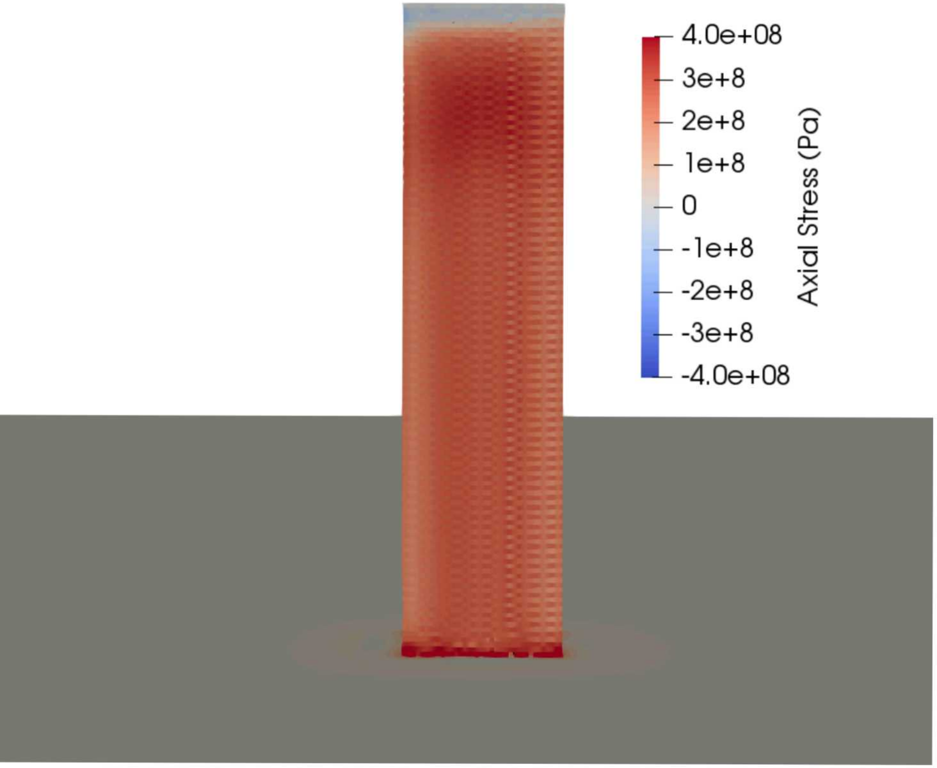

Mid-plane Cut View

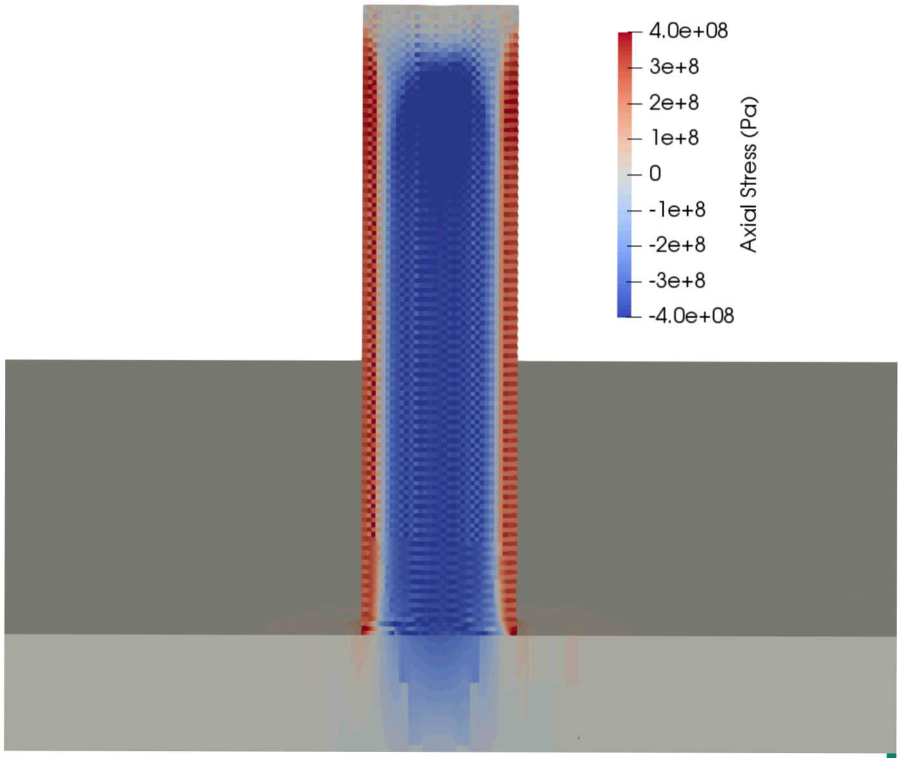

Model Captures Higher Yield but Under-Predicts Stress

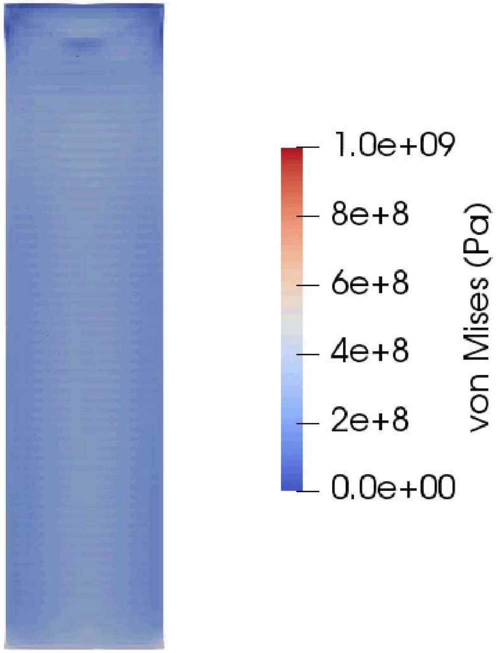

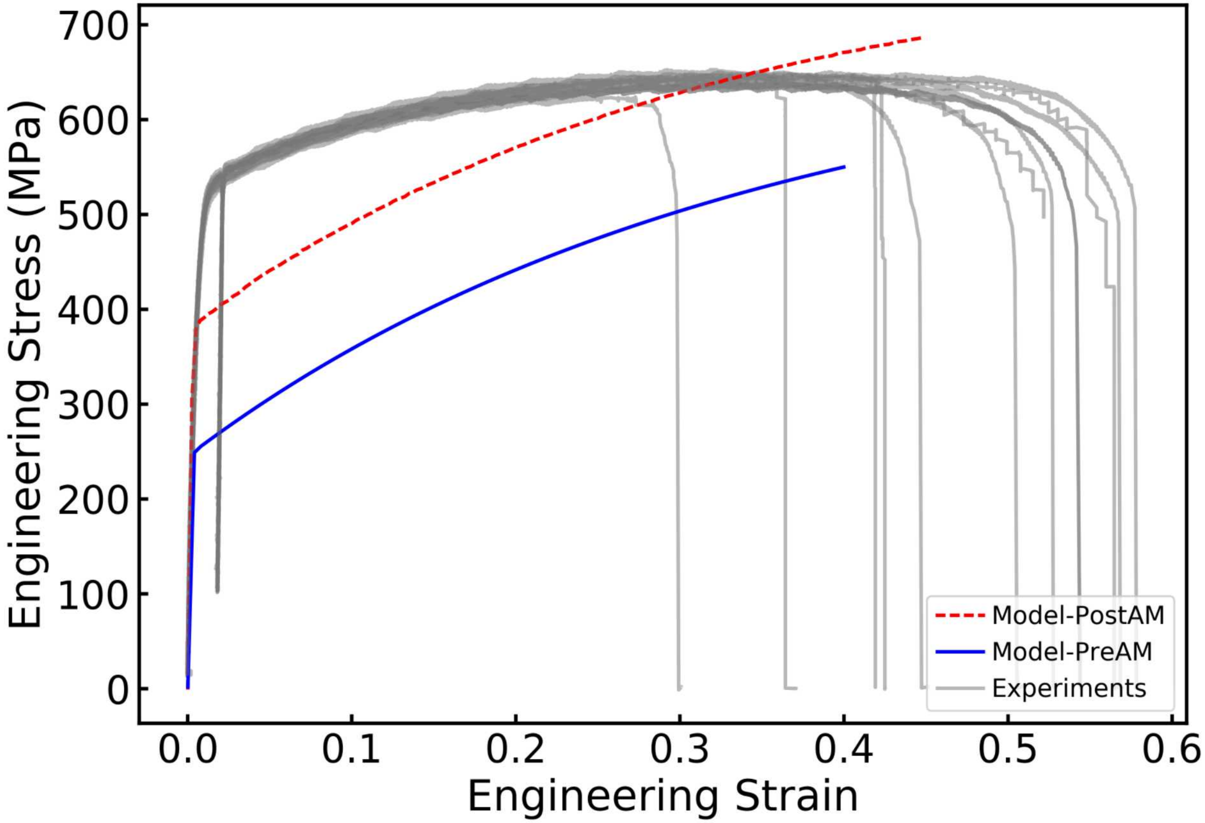

- Model with no residual stress was also simulated, but results were similar

Porosity Distribution is Directly Mapped to Mesh

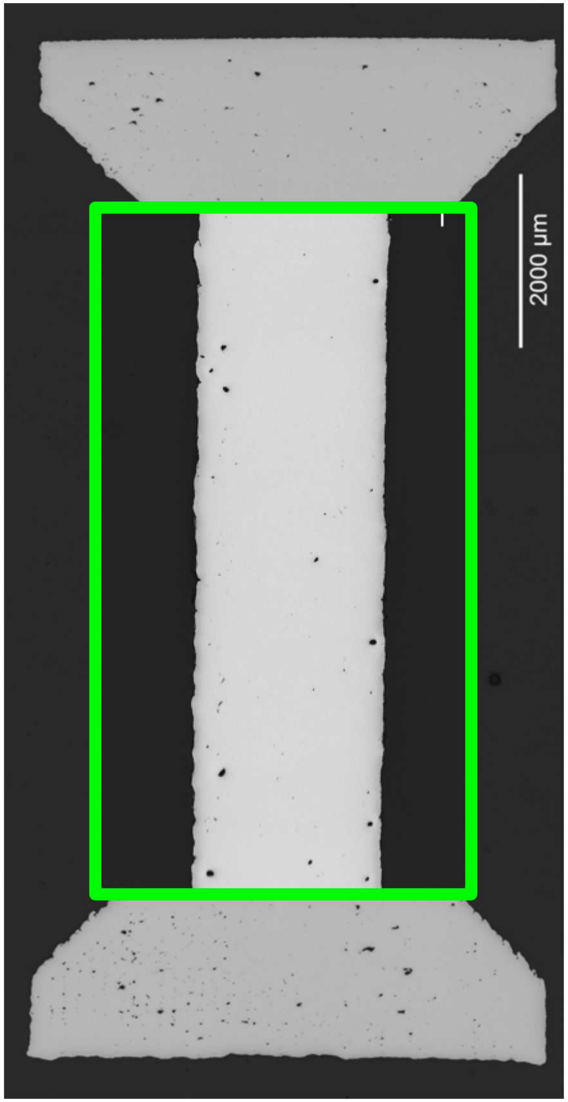

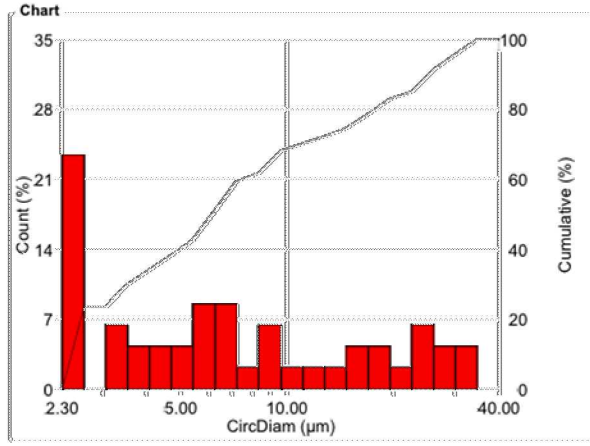

Porosity Mapping

x,y,z,r_{pore}

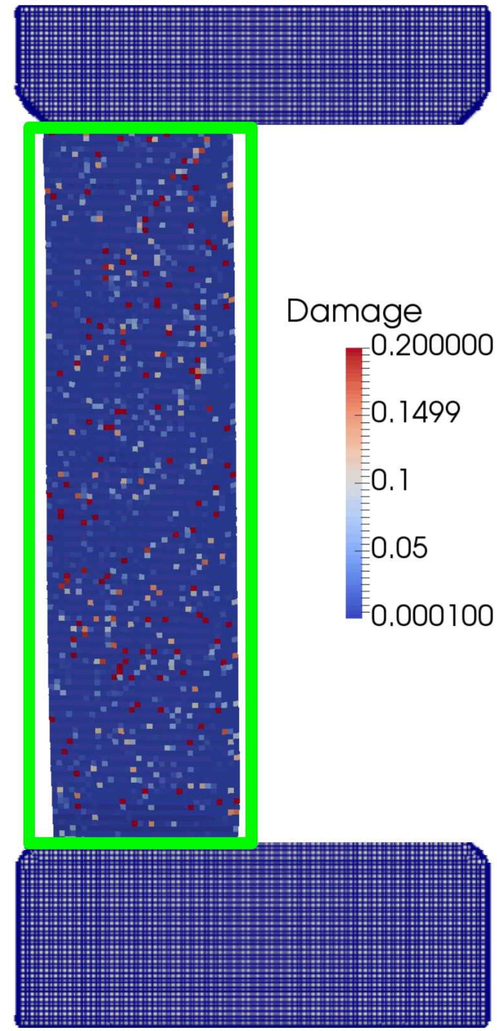

- Total Porosity: 2%
  - Sample distribution taken from 3rd Sandia Fracture Challenge

Tensile Results with Porosity

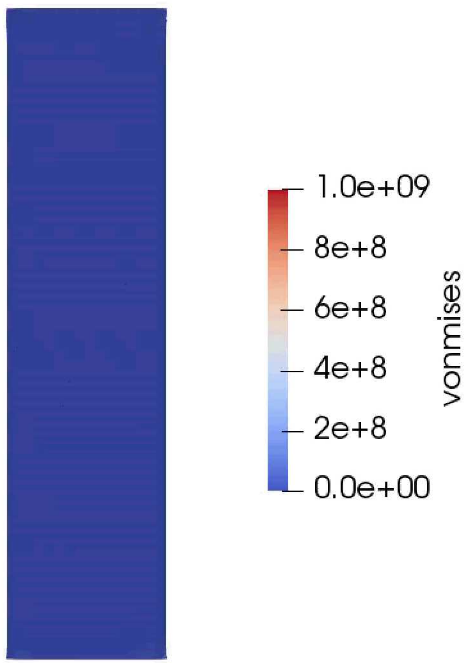

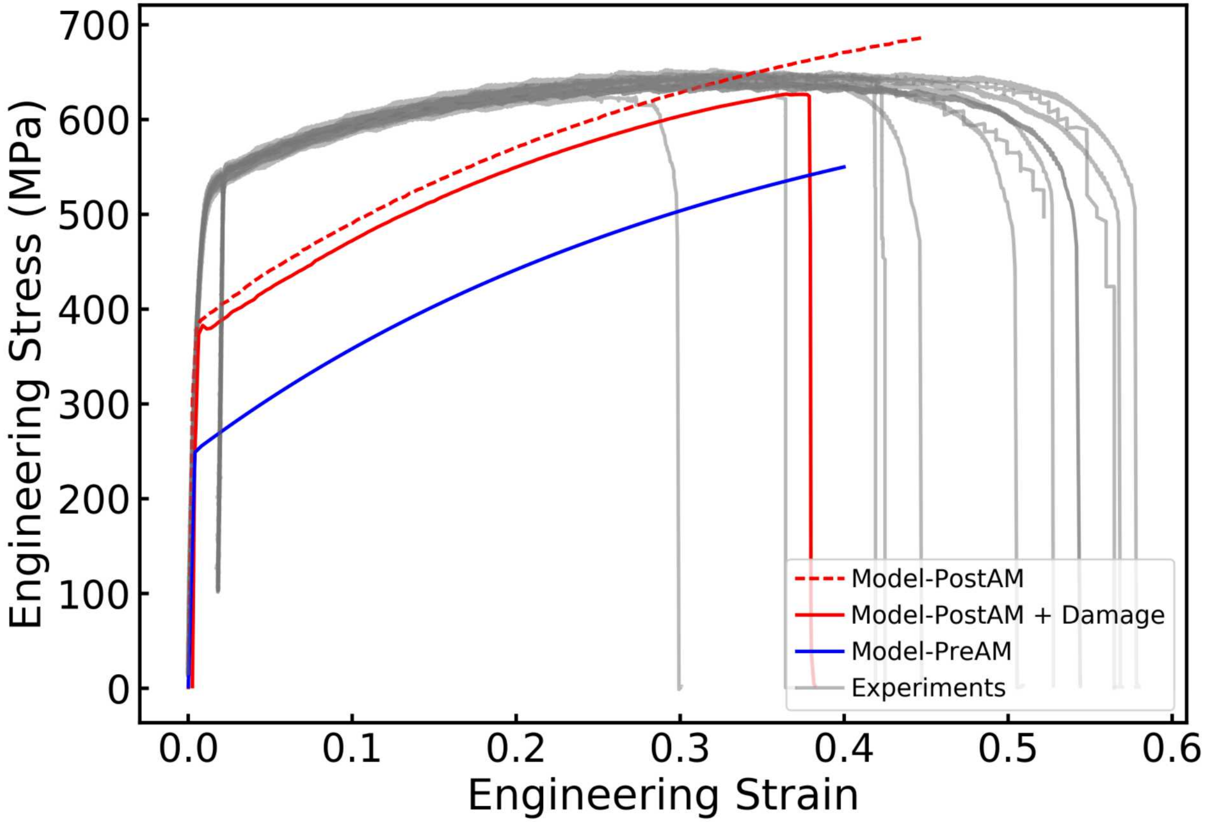

Laser Parameter Study

Running a parameter study over 3 levels of laser power and scan velocity, for a total of 9 runs.

This will result in a matrix which we can use to do a main effects study and also compare with data from the ProX machine

Initial step toward model validation

	Laser Power (W)		
Scan Velocity (m/s)	**100**	**110**	**125**
1.05			
1.4			
1.75			

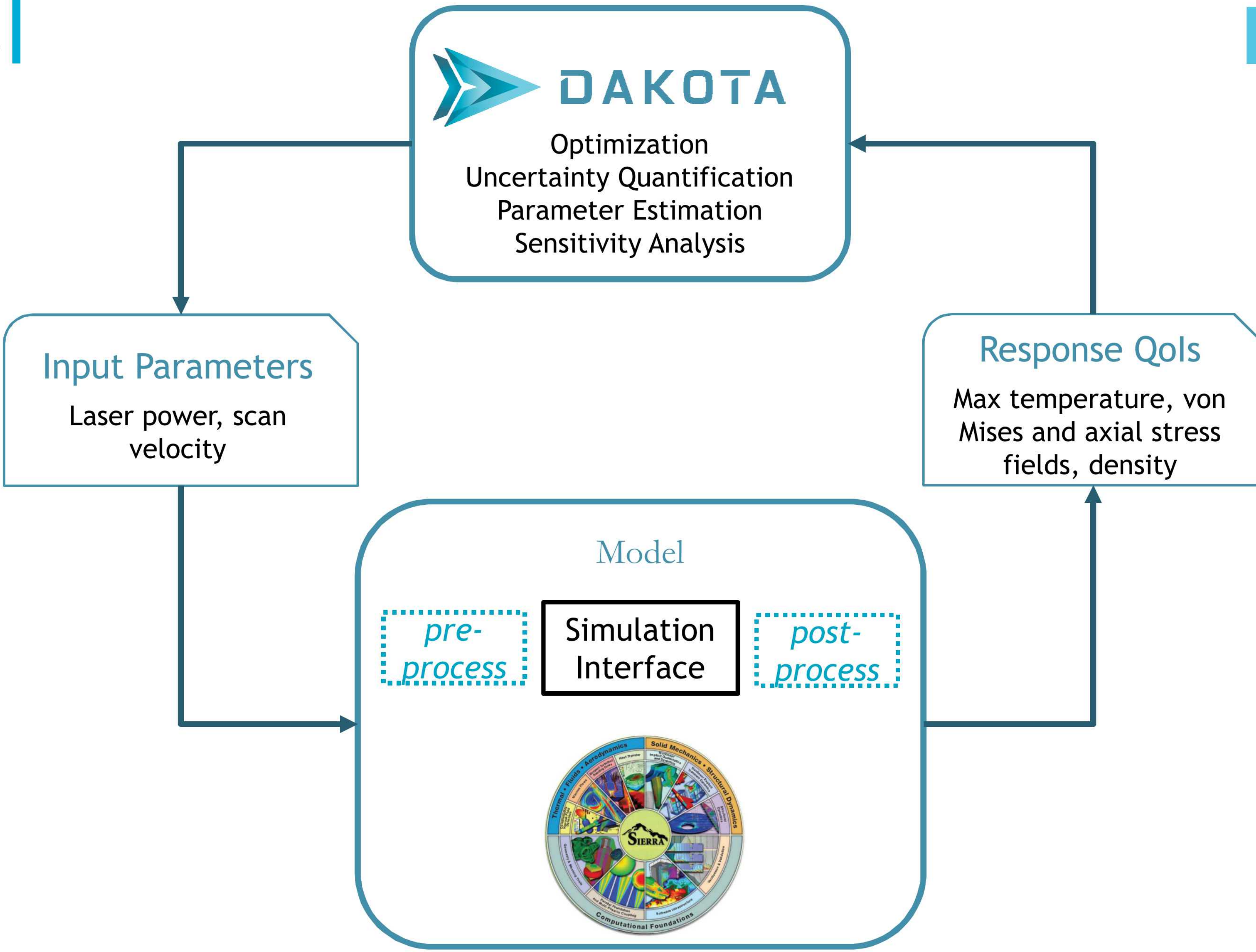
DAKOTA
Optimization
Uncertainty Quantification
Parameter Estimation
Sensitivity Analysis
Input Parameters
Laser power, scan velocity
Response QoIs
Max temperature, von Mises and axial stress fields, density
Model
pre-process
Simulation Interface
post-process
SIERRA
Computational Foundations

Correlation Results

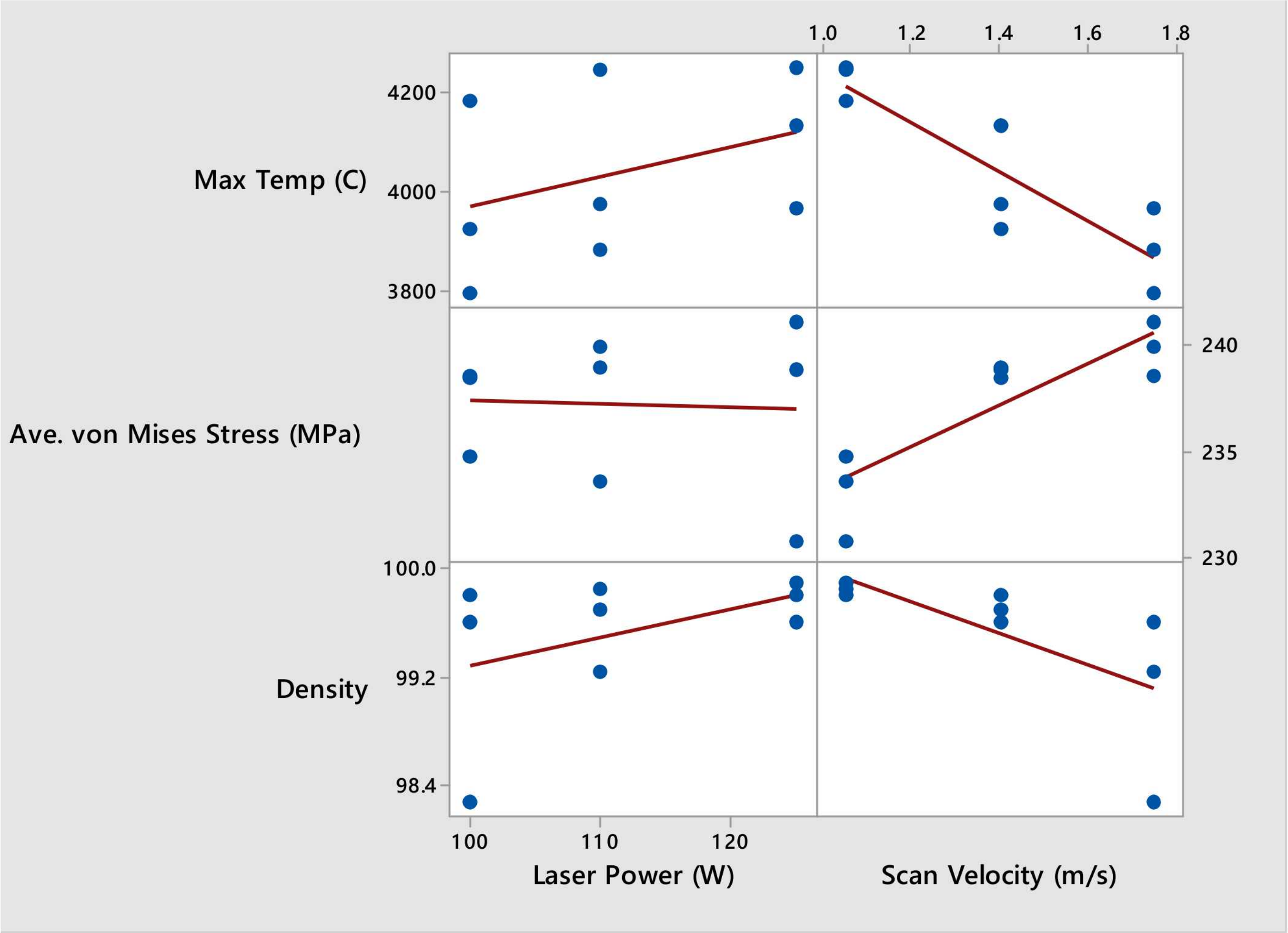

- Laser power is positively correlated to maximum temperature and density,
- Scan velocity is negatively correlated with temperature and density, and positively correlated with von Mises stress.

Yield Strength Predictions are Lower Than Experimental Results

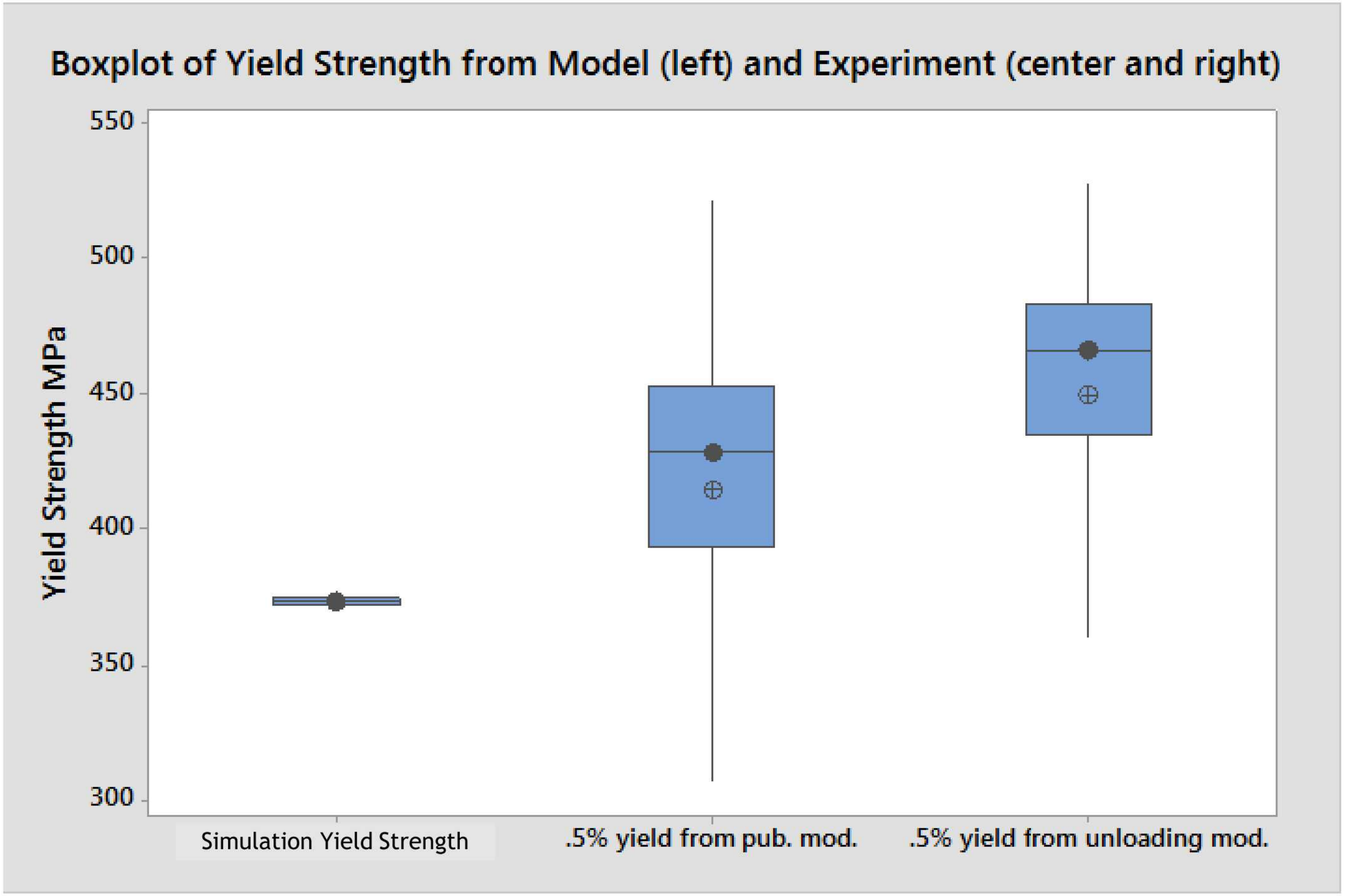

Max Temperature, Stress, and Density Appear to Show Higher Correlation to Scan Velocity

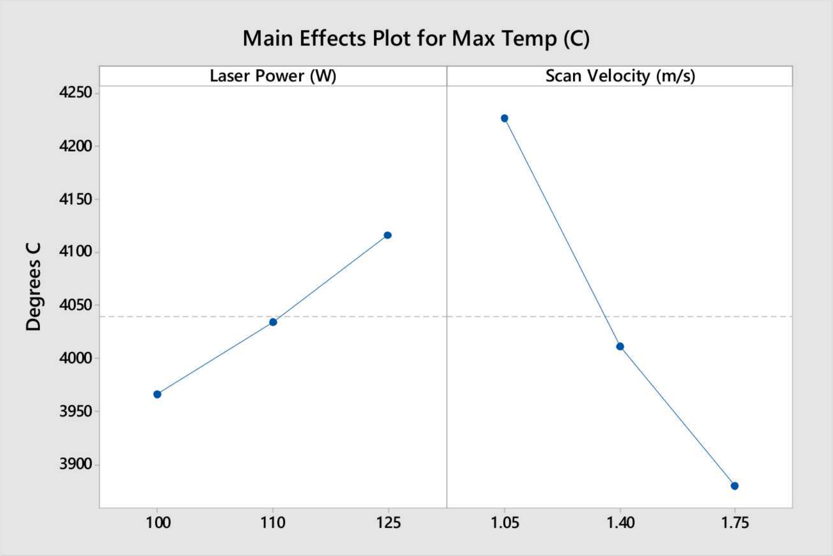

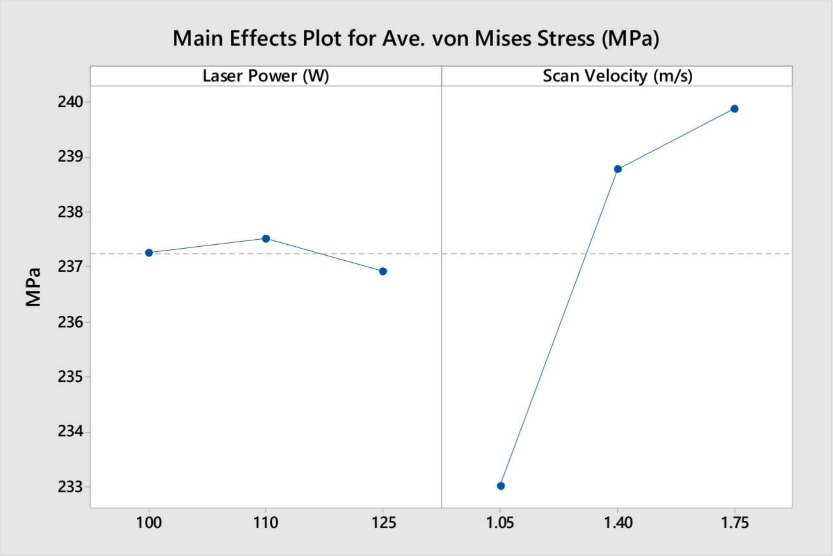

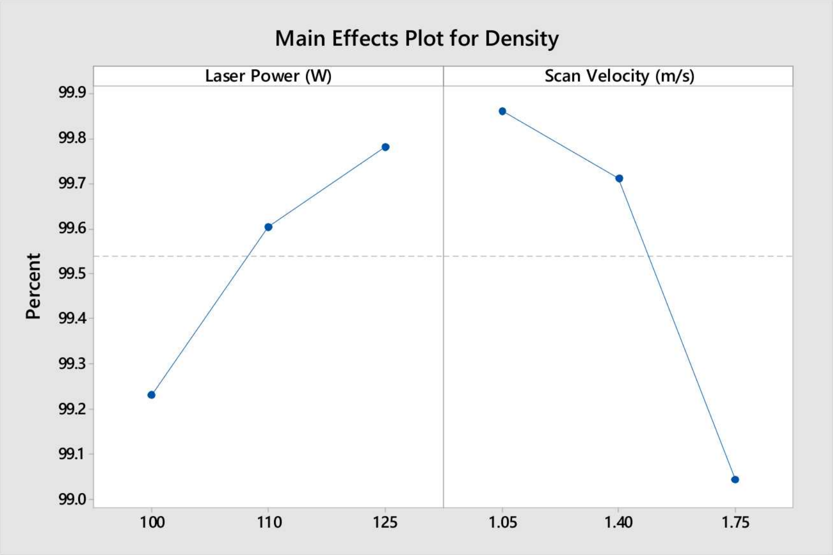

Conclusions

- Tensile specimen has been simulated to investigate P-S-P-P relationships
- Initial higher yield and decreased hardening is predicted
  - Yield predictions are too low, possibly due to incorrect high temperature assumptions
- Residual stress is predicted
- Damage variable provides a way to directly map defects to performance simulations
- Laser parameter study demonstrates initial step toward qualification
- Rich data set which shows some overall main effect trends that are as expected

Future Work – Property Prediction

- Refine material model at high temperatures with near melt Gleeble test data
- Run more realizations of porosity for UQ (only 1 shown)
- Simulate full dogbone
- Simulate heat treatments
- Predict microstructure for crystal plasticity comparison

Questions?

SNL Modeling Work

Codes
LAMMPS, SPPARKS,
Sierra/Aria,
Sierra/Adagio

Part Scale Thermal & Solid Mechanics
Kyle Johnson, Kurtis Ford, Mike Stender,
Lauren Beghini & Joe Bishop

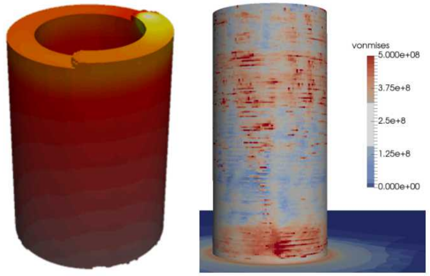

Mesoscale Thermal Behavior
Mario Martinez & Brad Trembacki

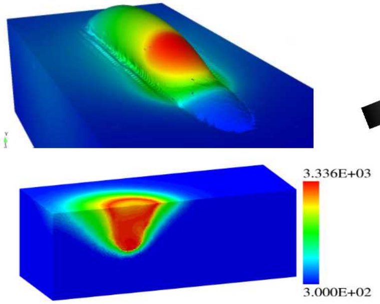

Powder Spreading
Dan Bolintineanu

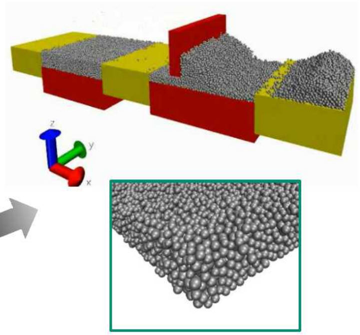

Part Scale Microstructure
Theron Rodgers

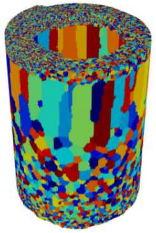

Powder Behavior
Mark Wilson

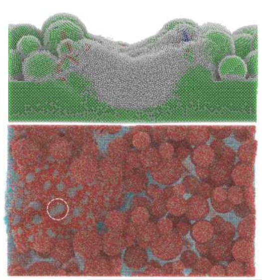

Mesoscale Texture/Solid Mechanics/CX
Judy Brown, Theron Rodgers and Kurtis Ford

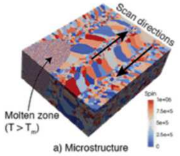

10^{-6} — 10^{-3} — 1

Length Scale (m)

Example: Full Tube Forming Process

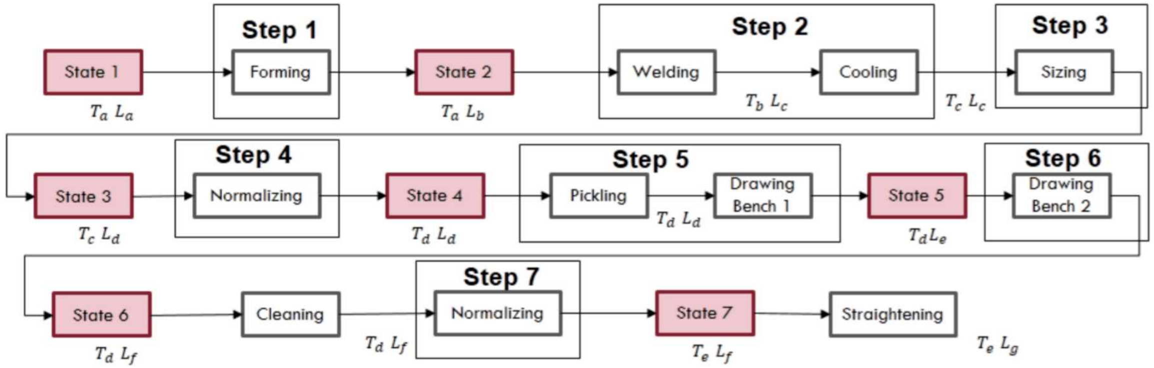

Microstructure

Ferrite grain size distribution
Ferrite area fraction
Carbide size and distribution
Carbide area fraction

Mechanical Properties

Vicker's hardness
Low strain rate tension/compression data
High strain rate tension/compression data
High temperature tension/compression data

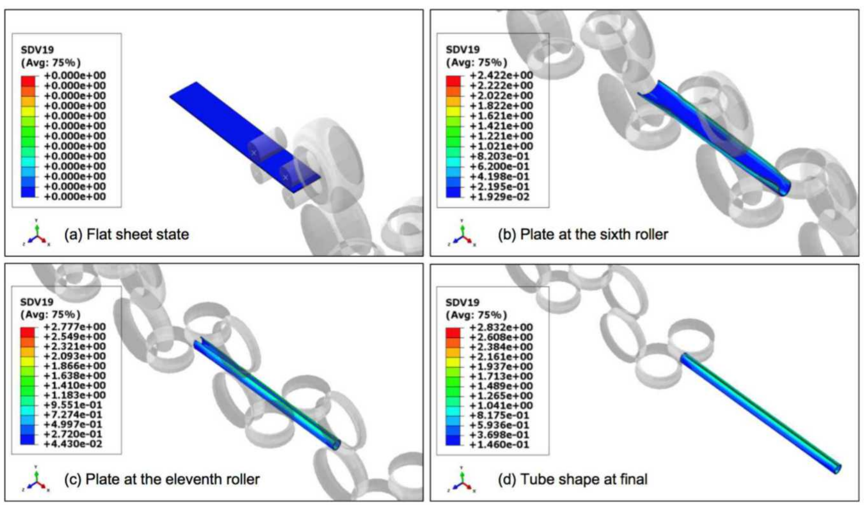

Figure 7.7. Tube forming simulation showing the plastic equivalent strain progression from sheet to tube.

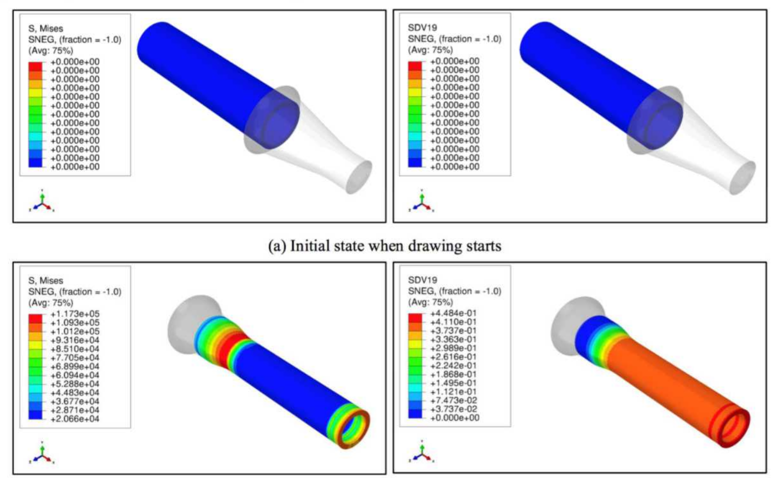

(a) Initial state when drawing starts

(b) Elongation of the tube by die

Figure 7.19. Second drawing simulation presenting von Mises stress (left, in Psi) and the equivalent plastic strain (SDV19, right) progressions. At this process, tube was significantly deformed due to small radius of the die.

H. Cho, Y. Hammi, D.K. Francis, T. Stone, Y. Mao, K. Sullivan, J. Wilbanks, R. Zelinka, and M.F. Horstemeyer. ICME book (in progress)
H. Cho *et al.*, "Finite Element Model for Plymouth Tube Processing using Internal State Variables", ICME 2015.

Model Showed Good Agreement at Each Step in Process

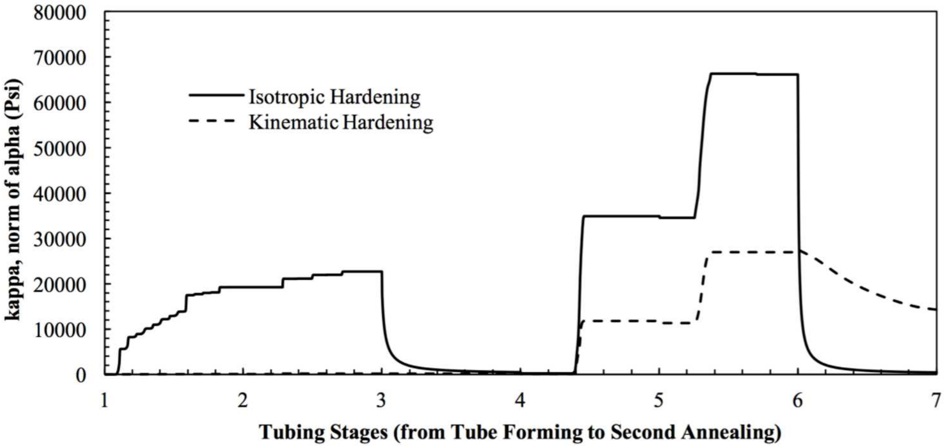

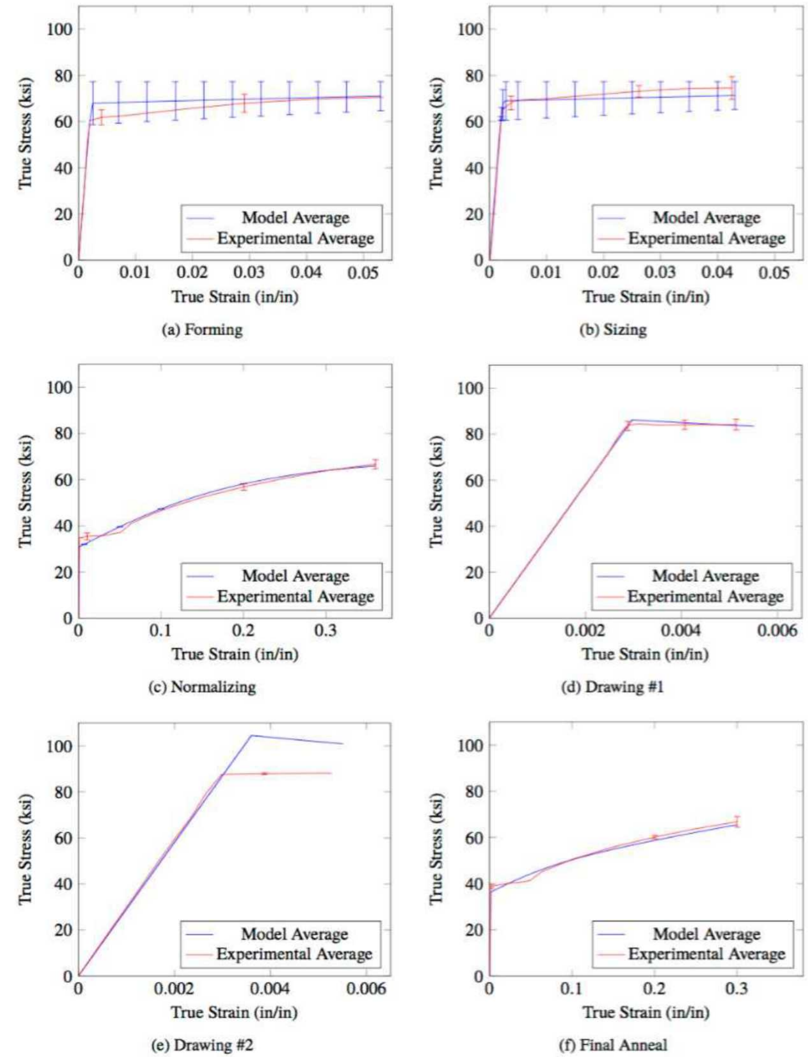

Figure 3 Stress-strain behavior comparison between simulation and experimental result (tension) after each step

- Model captures each process with one set of parameters calibrated for initial process
- Final mechanical properties are very close to experiment

H. Cho, Y. Hammi, D.K. Francis, T. Stone, Y. Mao, K. Sullivan, J. Wilbanks, R. Zelinka, and M.F. Horstemeyer. ICME book (in progress)

H. Cho *et al.*, “Finite Element Model for Plymouth Tube Processing using Internal State Variables”, ICME 2015.

Performance: Higher Yield Captured in 304L SS Upon Reloading

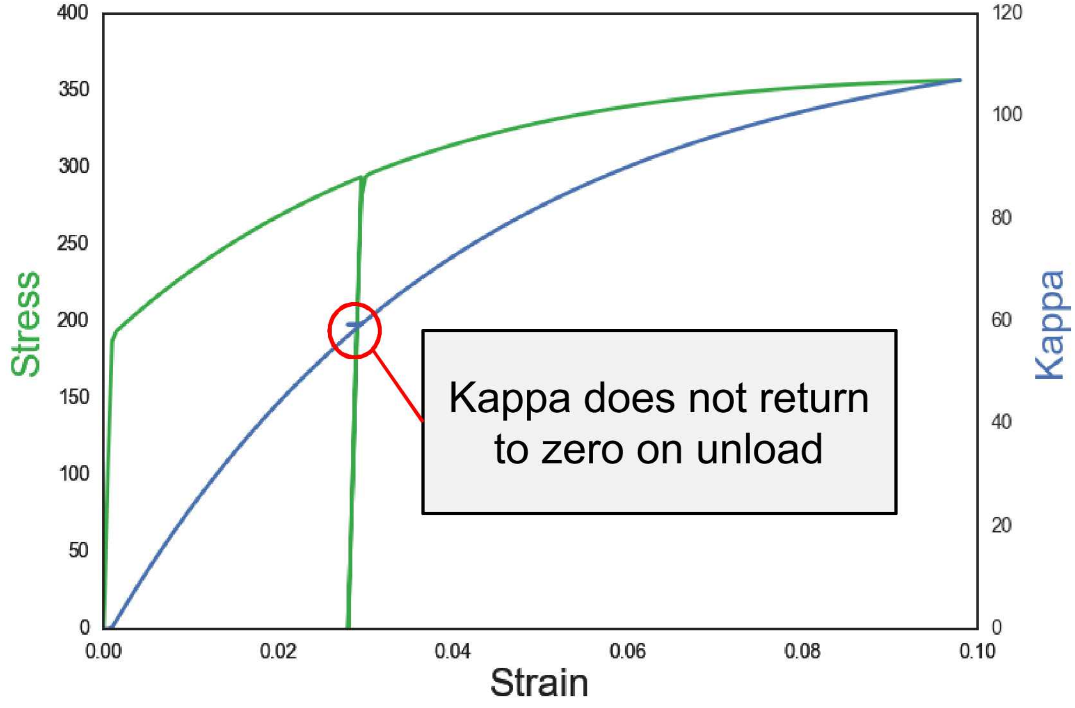

$$\dot{\kappa} = [H(\theta) - R_d(\theta)\kappa]\dot{\epsilon}_p$$

- Example: One element 304L SS loaded to 3 % strain, followed by unload and reload
- Model accurately captures loading history with kappa ISV

Process Setting Effects on Properties (Laura Swiler)

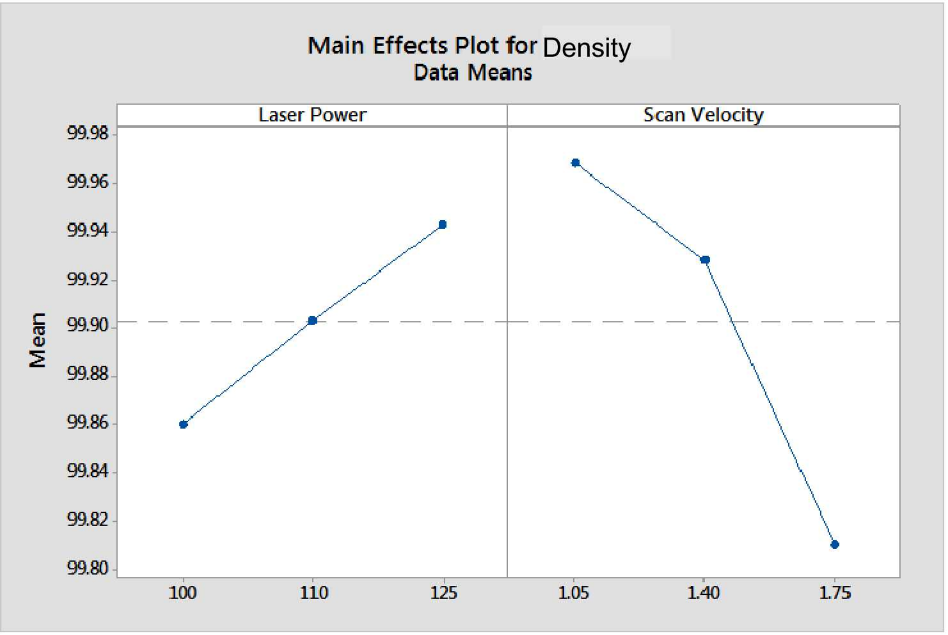

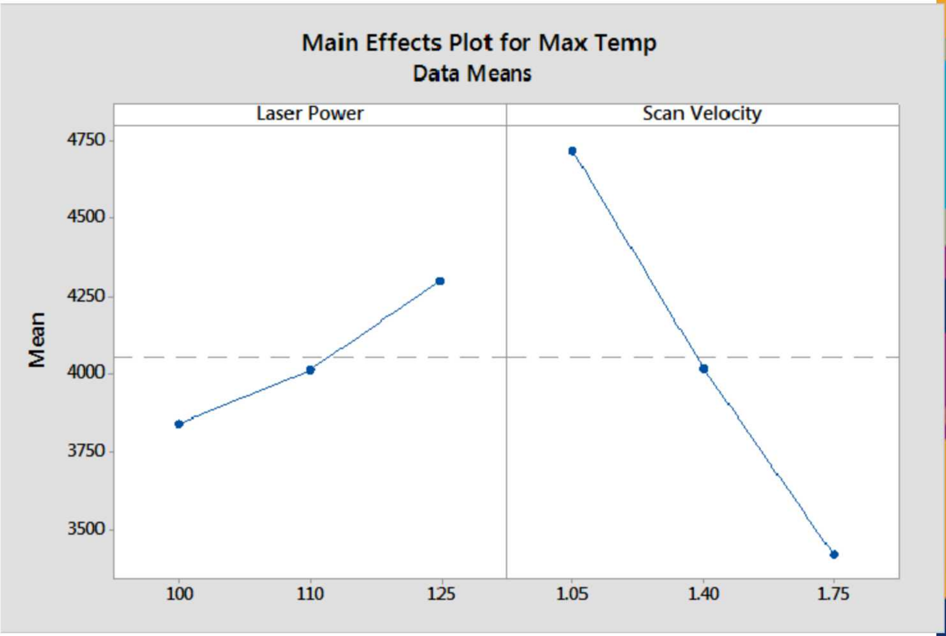

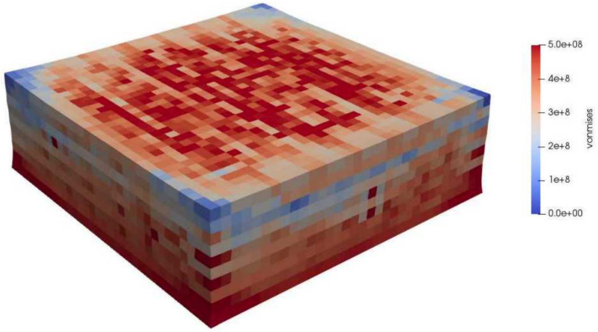

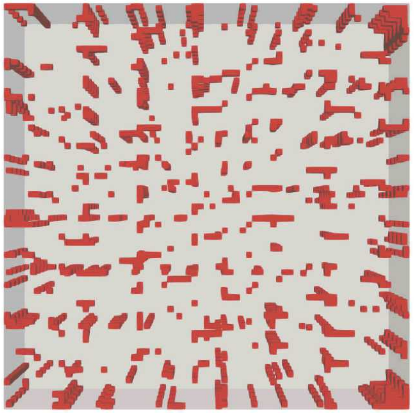

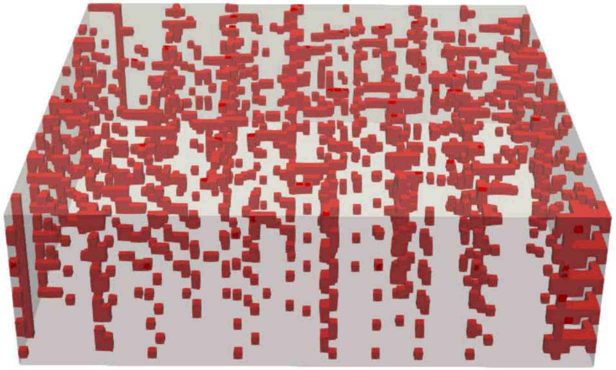

Thermal Modeling in Aria

$$\rho C_p \frac{\partial T}{\partial t} + \rho C_p \boldsymbol{v} \cdot \boldsymbol{\nabla} T = -\boldsymbol{\nabla} \cdot \mathbf{q} + H_V$$

Volumetric Gaussian Laser Heat Source

```
begin laser heating
  Activation Temperature = 1698
  power = 2000
  beam diameter = 4.2
  efficiency = 0.4
  path function = path
  depth direction = -z
  distribution = gaussian
  source type = activation_hemisphere
  spatial influence factor = 1.2
  add volume block_40
end
```

Radiation and Convection

$$\mathbf{q} = \varepsilon\sigma(T^4 - T_r^4)$$

$$\mathbf{q} = h(T - T_\infty)$$

Conduction

$$\mathbf{q} = -k\nabla T$$

Element Status	K Value $(W/(m * K))$
Inactive LENS	0
Inactive Powder Bed	Powder Property (< 1)
Active	Bulk Property

Material Addition in Aria